applied optics

Wavelength calibration model for prism-type echelle spectrometer by reversely solving prism's refractive index in real time

Rui Zhang,[1,2] Bayanheshig,[1,*] Lu Yin,[1,2] Xiaotian Li,[1] Jicheng Cui,[1] Jin Yang,[1] and Ci Sun[1]

[1]Grating Technology Laboratory, Changchun Institute of Optics and Fine Mechanics and Physics, Chinese Academy of Sciences, Changchun, Jilin 130033, China
[2]University of Chinese Academy of Sciences, Beijing 100049, China
*Corresponding author: bayin888@sina.com

Received 5 January 2016; revised 7 April 2016; accepted 12 April 2016; posted 13 April 2016 (Doc. ID 256833); published 17 May 2016

In an echelle spectrometer equipped with a prism cross-dispersion element, wavelength calibration is very difficult because of the complex, nonlinear interaction between the prism and the echelle grating. From the spectrometer geometry and the dispersion equations for the prism and the grating, a detailed mathematical model for wavelength calibration is derived that fits the refractive index of the prism in real time. An expression relating the refractive index, wavelength, and image coordinates is constructed, and standard wavelength sources and image positions are adopted to timely calculate the refractive index, which is affected by ambient factors such as temperature and air pressure. Experimental results indicate that the fitting accuracy of the refractive index in real time approaches 10^{-4}, while the wavelength accuracy approaches 10^{-3} nm for the entire spectral range. © 2016 Optical Society of America

OCIS codes: (050.0050) Diffraction and gratings; (120.0120) Instrumentation, measurement, and metrology; (120.4640) Optical instruments.

http://dx.doi.org/10.1364/AO.55.004153

1. INTRODUCTION

Echelle grating spectrometers can analyze an entire spectrum at once and thus have many applications. The echelle grating enables high resolution, high diffraction efficiency and a broad spectral range [1–5]. However, overlapping diffraction orders appear in the dispersion, hindering the analysis of the spectrum. To eliminate order overlapping, a cross-dispersion element (prism or grating) is used to produce a two-dimensional spectrum on the detector. Due to the characteristic blazing of gratings, an echelle spectrometer with a cross-dispersion grating exhibits low optical efficiency and substantially uneven dispersion at different wavelengths. Thus, spectral overlap cannot be eliminated. A prism can avoid these problems entirely [6], and thus prisms are generally preferred as cross-dispersion components [7–10].

Algorithms for echelle spectrometer wavelength calibration are very active research areas. The procedure for wavelength calibration is very straightforward for spectrometers equipped with grating cross-dispersion elements and can be refined with mathematical models [11]. However, when a prism is used, its interaction with the echelle grating is very complex and nonlinear. Calibration is made even more difficult by the wavelength dependence of the prism's refractive index. Moore and Furst [12] used a prism cross-dispersion element as a separate spectrometer behind an echelle spectrometer and then used a low-order polynomial to calibrate the wavelength according to the optical geometry of the two spectrometers. Unfortunately, when the prism spectrometer was set inside the echelle spectrometer, the method failed. Sadler and Littlejohn [13] formulated a polynomial for the temperature dependence of the refractive index, but ignored the effects of humidity and pressure, which will change the refractive index [14,15].

Here, a new model is presented for wavelength calibration of prism-type echelle spectrometers that is based on real-time fitting of the prism's refractive index. The mathematical model reduces cross-dispersed echelle spectra according to the geometry of the spectrometer. Next, the relationship between the refractive index and the geometrical parameters is confirmed according to the model, completing an inverse solution of the refractive index. Finally, the refractive index fits are substituted into the mathematical model for the wavelength calibration. The refractive index of the prism can be fitted accurately in real time, insuring accurate wavelength calibration of the spectrometer.

2. MATHEMATICAL MODEL

The optical geometry of a prism-type echelle spectrometer in this paper is shown in Fig. 1 (in our case, the focal length is 321 mm).

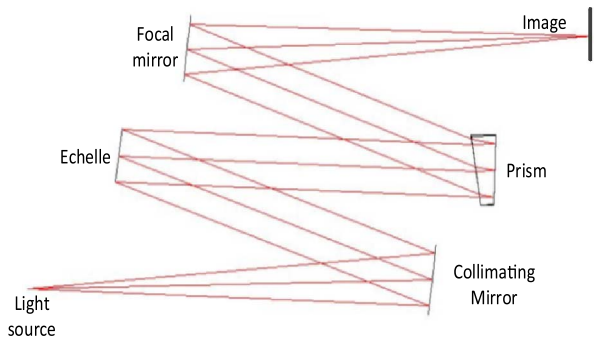

Fig. 1. Optical geometry of a prism-type echelle spectrometer.

The image position of the blaze wavelength in the center of the image plane; the diffraction angle of the grating is determined by

$$\theta_i = \theta_0 + \frac{y_i}{f\cos\omega}, \qquad i = 1, \ldots, p, \tag{1}$$

where θ_0 is the blaze angle, θ_i is the diffraction angle in the primary dispersion direction, y_i is the distance between an arbitrary image point and a point in the image center of the dispersion direction, f is the focal length of the spectrometer, and ω is the grating offset angle. p is the pixel number of the CCD-array detector in the y direction.

The conical diffraction equation of the echelle grating can be simplified to

$$d(\sin i + \sin\theta_i)\cos\omega = m_j\lambda, \qquad j = 1, \ldots, q, \tag{2}$$

where d is the groove spacing, i is the incidence angle, m_j is the diffraction order, ω is the grating offset angle, and λ is the incident wavelength. q is the number of diffraction orders.

By substituting Eq. (1) into Eq. (2), we obtain

$$\lambda = \frac{d}{m_j}\left[\sin i + \sin\left(\theta_0 + \frac{y_i}{f\cos\omega}\right)\right]\cos\omega. \tag{3}$$

Assuming a CCD-array detector has an array of $N \times N$ pixels with size α, the he Y positions of any incident wavelength focused onto the array are given by

$$Y_i = \frac{y_i}{a} + \frac{N}{2}, \tag{4}$$

where Y_i are the image coordinates on the CCD array.

From Eqs. (3) and (4), we know that λ is a function of Y_i and m_j. The matrix can be built according to the relationship among λ, Y_i, and m_j. Y_i is the line number, and m_j is the row number. The elements of the matrix are the wavelength calculated by Eqs. (3) and (4)

$$\lambda_{Y,m} = \begin{bmatrix} \lambda_{Y_1m_1} & \lambda_{Y_1m_2} & \cdots & \lambda_{Y_1m_q} \\ \lambda_{Y_2m_1} & \lambda_{Y_2m_2} & \cdots & \lambda_{Y_2m_q} \\ \cdot & \cdot & \cdot & \cdot \\ \cdot & \cdot & \cdot & \cdot \\ \lambda_{Y_pm_1} & \lambda_{Y_pm_1} & \cdots & \lambda_{Y_pm_q} \end{bmatrix}. \tag{5}$$

If we place the Y coordinate into the corresponding wavelength position, the matrix of the Y_i coordinates is

$$Y_{Y,m} = \begin{bmatrix} Y_{Y_1m_1} & Y_{Y_1m_2} & \cdots & Y_{Y_1m_q} \\ Y_{Y_2m_1} & Y_{Y_2m_2} & \cdots & Y_{Y_2m_q} \\ \cdot & \cdot & \cdot & \cdot \\ \cdot & \cdot & \cdot & \cdot \\ Y_{Y_pm_1} & Y_{Y_pm_1} & \cdots & Y_{Y_pm_q} \end{bmatrix}. \tag{6}$$

The relationships among the y-axis coordinates, the wavelengths, and the diffraction order can be established by Eqs. (1)–(5), and the matrix can be built as Eq. (6). Next, we deduce the expressions relating to the x-axis coordinates, the y-axis coordinates, and the diffraction order.

Figure 2 depicts light propagation from the prism to the parabolic mirror and onto the image plane in the echelle spectrometer. L_0 is the light line that reaches the parabolic mirror (point A is the intersection) and the center of the image plane (point B is the intersection). If the center coordinate of the image plane is set to zero, then an arbitrary light line L performs parallel motion from point A' to the point A, and the image coordinate is X. If the angle between L and L_0 is δ and the focal length of the parabolic mirror *is* f, then the image coordinate X is given by

$$X = f^* \tan\delta. \tag{7}$$

The angle between L and L_0 can be acquired from

$$\delta = \beta_1 - \beta_0, \tag{8}$$

where β_1 and β_0 are the output angles of the light lines L and L_0 at the prism, respectively. L_0 is the light line that reaches the image center of the CCD. β_0 can be deduced through geometrical optics and is constant so λ_0 is constant as well.

The output angle from the prism of arbitrary light can be expressed as

$$\sin\beta = n(\lambda)\sin[2d_m - \sin^{-1}\alpha/n(\lambda)]. \tag{9}$$

From Eqs. (7)–(9), we obtain

$$X = f^*\tan\{\arcsin\{n(\lambda_1)\sin[2d_m - \sin^{-1}\alpha/n(\lambda_1)]\} - \arcsin\{n(\lambda_0)\sin[2d_m - \sin^{-1}\alpha/n(\lambda_0)]\}\}, \tag{10}$$

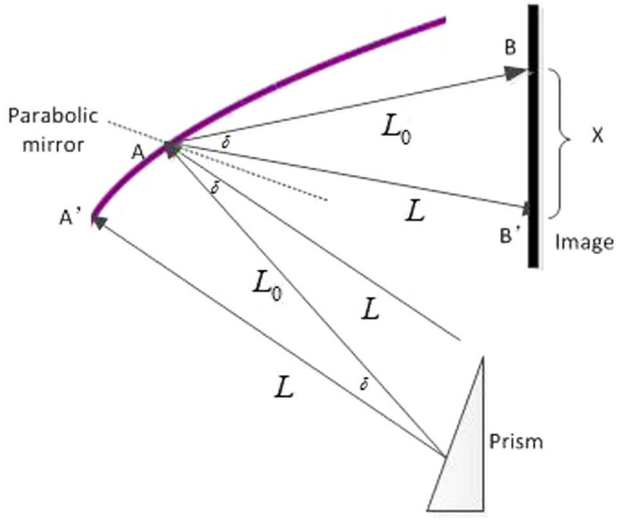

Fig. 2. Schematic of light propagation from the prism and the parabolic mirror to the image plane.

where λ_1 and λ_0 are the wavelengths with output angles β_1 and β_0, respectively; α is the incidence angle of the prism; d_m is the apex angle of the prism; and $n(\lambda)$ is the wavelength-dependent refractive index.

Generally, there are three expressions for the relationship between refractive index and wavelength, separately named as the exponential decay, the Cauchy distribution, and the Sellmeier method [16,17] shown, respectively, in Eqs. (11)–(13):

$$n = A + B^* \exp\left(\frac{-\lambda}{C}\right), \tag{11}$$

$$n = A + \frac{B}{\lambda^2} + \frac{C}{\lambda^4}, \tag{12}$$

$$n^2 = A + \frac{B}{\lambda^2 - C} - D\lambda^2, \tag{13}$$

where n is the refractive index for wavelength λ, and A, B, C, and D are coefficients. According to experimental analysis, Eq. (13) has the most accurate fit for the refractive index. Thus, it will be used the following.

From Eqs. (3)–(13), we can formulate the coordinates X_i and Y_j and the diffraction order m as follows:

$$X_{Y,m} = \begin{bmatrix} X_{Y_1 m_1} & X_{Y_1 m_2} & \cdots & X_{Y_1 m_q} \\ X_{Y_2 m_1} & X_{Y_2 m_2} & \cdots & X_{Y_2 m_q} \\ \cdot & \cdot & \cdot & \cdot \\ \cdot & \cdot & \cdot & \cdot \\ X_{Y_p m_1} & X_{Y_p m_1} & \cdots & X_{Y_p m_q} \end{bmatrix}. \tag{14}$$

According to Eqs. (5), (6), and (14), the matrix about λ, X_i, and Y_j can be expressed as Eq. (15)

$$\lambda_{X,Y} = \begin{bmatrix} \lambda_{X_1 Y_1} & \lambda_{X_1 Y_2} & \cdots & \lambda_{X_1 Y_q} \\ \lambda_{X_2 Y_1} & \lambda_{X_2 Y_2} & \cdots & \lambda_{X_2 Y_q} \\ \cdot & \cdot & \cdot & \cdot \\ \cdot & \cdot & \cdot & \cdot \\ \lambda_{X_p Y_1} & \lambda_{X_p Y_1} & \cdots & \lambda_{X_p Y_q} \end{bmatrix}. \tag{15}$$

Assuming a constant refractive index, we call this method the initial refractive index method. In short, the steps for wavelength calibration are as follows: (1) We calculate the corresponding Y position for arbitrary wavelength with Eqs. (3) and (4). (2) We choose even wavelengths from glass catalogs, then use seven sets of wavelength data and the relational expression between refractive index and wavelength [e.g., Eq. (13)] to fit coefficients such as A, B, C, and D in Eq. (13). Finally, we can confirm the initial expression of the refractive index and wavelength. (3) By substituting the initial expression of the refractive index and wavelength into Eq. (10), we can calculate the corresponding X position for the arbitrary wavelength.

Because the prism's refractive index is the most important factor that determines the accuracy of the wavelength calibration, the above "initial refractive index method" is not recommended; instead, the true refractive index should be acquired for each wavelength calibration in time. Standard refractive index measurements require an extra optical path [18] and cannot be performed in real time. Ambient changes in temperature, humidity, and pressure will decrease the accuracy of the calculated image-plane coordinates and wavelengths.

Therefore, we calculate the refractive index in real time with our model and then use it to fit the detailed relational expression between wavelength and refractive index. The accuracy of the wavelength calibration is improved by substituting the fitted refractive index expression into the model.

The steps of our method thus are as follows: (1) The corresponding Y position of an arbitrary wavelength is exactly calculated, and the corresponding X position is roughly approximated by the initial refractive index method. (2) Since the wavelength values of the standard light source are known, the corresponding Y and X values are calculated by the initial refractive index method. Next, we can find the corresponding light spot from spectrogram according to the Y and X values calculated by the initial refractive index method. Finally, the accurate X position can be read out by the software of the CCD detector. (3) The accurate refractive index at X is calculated with Eq. (10). We now know the characteristic wavelength and the corresponding accurate refractive index. (4) We then obtain the accurate relationship between refractive index and wavelength [such as in Eqs. (11)–(13)] by fitting. Thus, we can acquire the refractive index for arbitrary wavelength λ by the accurate expression $n(\lambda)$. (5) We substitute that exact expression into Eq. (10) and confirm the X position in the image plane for arbitrary wavelength λ. By doing all the above steps, we can acquire the X_i and Y_j coordinates in the image plane for arbitrary wavelength λ and complete the calibration process. If we know the image coordinates from the spectrogram, the corresponding wavelengths at those coordinates can be calculated.

3. EXPERIMENTAL ANALYSIS

A. Inverse Solution of Refractive Index

In a prism-type echelle spectrometer, the prism is used to coarsely resolve the light along the x axis, while the echelle provides high spectral resolution along the y axis. Figure 3 shows the calculated results of the wavelength calibration. The highlighted lines represent incident rays at specific positions with values corresponding to wavelength. The wavelength increases from left to right; thus, the wavelengths are continuous along the y axis, and discontinuous along the x axis. The Y positions are accurately calculated with Eqs. (3) and (4). Therefore, when the error of the X position is less than half the distance of a pixel between two adjacent wavelengths along the x axis, the wavelength can be accurately calculated.

According to the model, the wavelength becomes shorter when the distance in pixels between two adjacent wavelengths along the x axis becomes longer (see Fig. 3). The longest distance is 10 pixels, and the shortest is 2 pixels (see Fig. 4). Thus, as stated above, when the error in the X position is less than one pixel, the wavelength calibration model is accurate. Thus, the precision requirement of wavelength calibration can be met when the error in the refractive index is ≤ 0.0004.

To verify the fitting precision of the refractive index, we acquired spectra for Hg (see Fig. 5), Zn, Fe, Bi, and Se lamps with the echelle spectrometer. Figure 5 is the two-dimensional spectrum of an Hg lamp acquired by the CCD-array detector, which has an array of 1204×1024 pixels with a size of 13 μm.

Thirty-two sets of corresponding X and Y positions for different lamp wavelengths were extracted. Sixteen of those sets

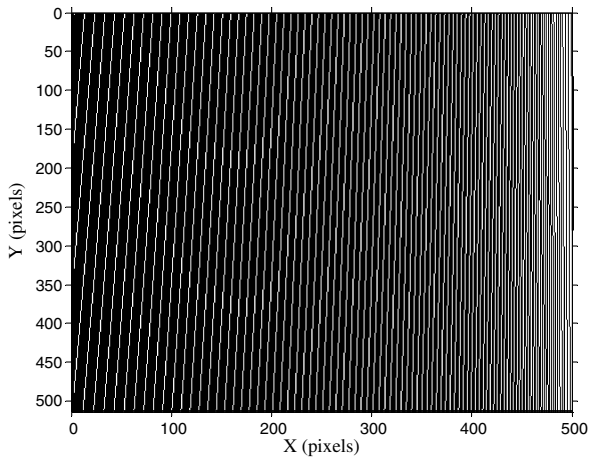

Fig. 3. Result of wavelength calibration model.

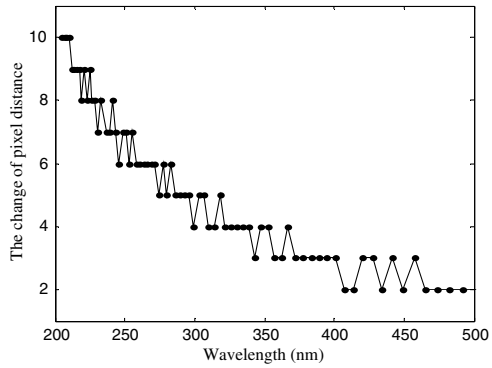

Fig. 4. Distance change in pixels between two adjacent wavelengths along the x axis.

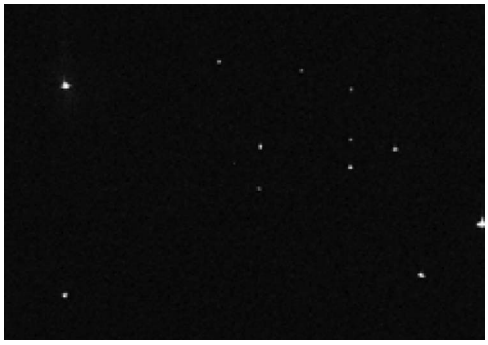

Fig. 5. Two-dimensional spectrum of a Hg lamp.

were selected to be fitting data; from these, $k(3 \le k \le 16)$ sets of data were selected. Following the steps of our method (1)–(5), evaluations of Eqs. (11)–(13) were calculated. At the same time, characteristic wavelengths from these k sets of data were substituted into Eqs. (11)–(13) to compute the refractive indices. Standard refractive indices are also calculated using X positions from the k sets and Eq. (10). Then, the results of the fitted refractive indices are compared with the ideal values

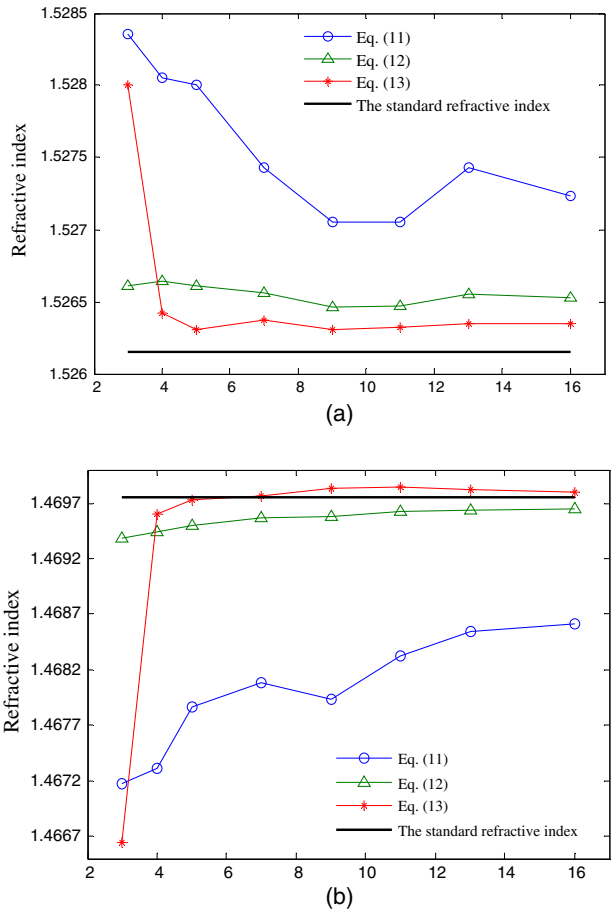

Fig. 6. Comparison of fitted and ideal refractive indices. (a) $\lambda = 223.061$ nm and (b) $\lambda = 404.656$ nm.

calculated by Eqs. (11)–(13). Figure 6 shows the comparison of calculations for the characteristic wavelengths of 223.061 and 404.656 nm. From Fig. 6, the errors between the fitted refractive indices and the ideal values decrease with increasing k. When the number of data sets exceeds five, the fitted refractive index converges. In addition, the maximum deviation between the fitted and ideal refractive indices calculated by Eqs. (11)–(13) are 0.001, 0.0004, and 0.0003, respectively. After comparison, Eq. (13) has the best fitting accuracy for the refractive index and meets the precision requirement of wavelength calibration.

B. Accuracy Validation of the Wavelength Calibration Model

Accurate image coordinates are prerequisite and foundational the wavelength calibration. The pixel deviation expresses the accuracy of the wavelength calibration model. Only if the pixel deviation is small enough will the wavelength calculation be accurately finished. The other 16 sets of data from the above 32 sets are used as test data to verify the X-position computation accuracy. By substituting the initial and fitted refractive indices into Eq. (10), the X positions are calculated. Figure 7 shows the errors between the ideal and calculated X positions. The maximum deviations for X positions

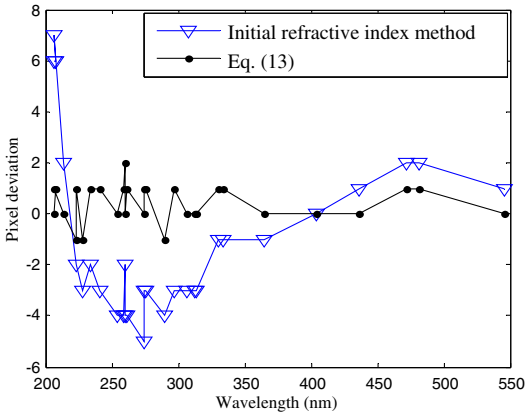

Fig. 7. Pixel deviations calculated by different methods.

computed with the initial refractive index and with Eq. (13) are 13 and 1 pixels, respectively. Figures 6 and 7, respectively, show that the refractive indices and the X positions fitted by Eq. (13) are the most accurate. The maximum pixel deviation error calculated by Eq. (13) is less than the pixel distance between two adjacent wavelengths along the x axis. Therefore, the wavelength along the x axis can be extracted without error. When Eq. (13) is used to fit the refractive index, the effect of X-coordinate error is negligible.

To verify the accuracy of this method, we also measured the continuous spectrum of a deuterium lamp. Figure 8 compares the ideal X positions from the lamp spectrum with those calculated with Eq. (13). Note that the deviation stays within one pixel.

After the X and Y positions are calculated, the wavelength calibration model is complete, and the incident wavelengths can be determined from the image coordinates. This can be used to analyze the accuracy of the wavelength calibration model. Figure 9 shows the deviation between the ideal wavelength and that calculated by the initial refractive index method. It also shows the deviation between ideal wavelength and that calculated by the proposed method. The extracted accuracies for the initial refractive index method and the proposed method are 10 nm and 5.2×10^{-3} nm, respectively. The accuracy of the wavelength calibration by the proposed method is thus 1900 times better than initial refractive index method.

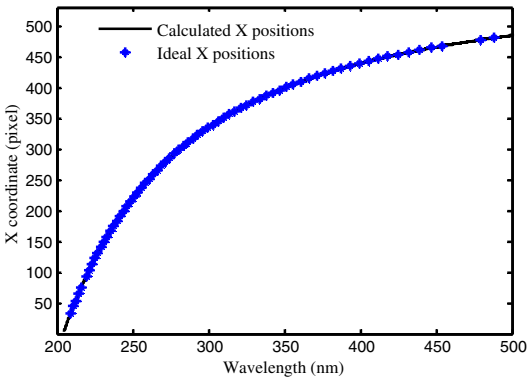

Fig. 8. Ideal and calculated X positions for a deuterium lamp.

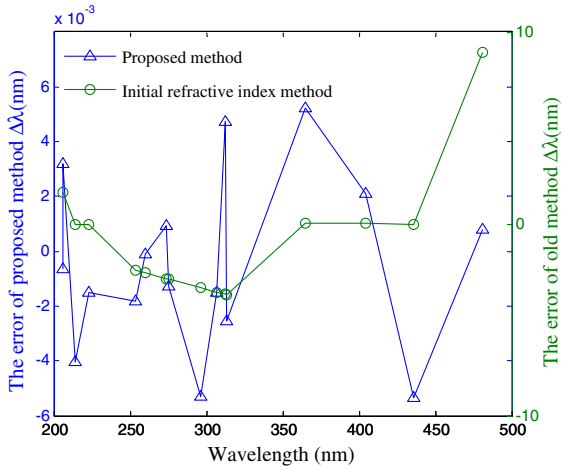

Fig. 9. Deviations of wavelength calibration by different methods.

4. CONCLUSION

A new method of wavelength calibration for prism-type echelle spectrometers is based on real-time fitting of the prism's refractive index. The wavelength calibration model is formulated by using the optical geometry of the spectrometer and the dispersion equations for the echelle and prism. The inverse solution of the refractive index is found by deriving the relationship between the refractive index and the X position in the CCD-array detector. In this way, the relationship between refractive index and wavelength is confirmed and utilized to improve the accuracy of wavelength calibration. The advantage of this method is that the refractive index can be fully determined in real time in the spectrometer, without other auxiliary equipment. The accuracy of the wavelength calibration by the proposed method is 1900 times better than that performed by the initial refractive index method, which assumes a constant refractive index. The proposed method has an accuracy approaching 10^{-3} nm for the entire spectral range of the spectrometer.

Funding. National Major Scientific Instrument and Equipment Development Projects (2014YQ120351); Chinese Finance Ministry for the National R&D Projects for Key Scientific Instruments (ZDYZ2008-1); National Natural Science Foundation of China (NSFC) (61505204); Ministry of National Science and Technology for National Key Basic Research Program of China (2014CB049500); Changchun Science and Technology Project (12ZX23); Jilin Major Province Science & Technology Development Program Project (20140203011GX).

REFERENCES

1. S. V. Bykov and B. Sharma, "High-throughput, high-resolution echelle deep-UV Raman spectrometer," Appl. Spectrosc. **67**, 873–883 (2013).
2. O. Korablev and F. Montmessin, "Compact echelle spectrometer for occultation sounding of the Martian atmosphere: design and performance," Appl. Opt. **52**, 1054–1065 (2013).
3. M. P. Wood and J. E. Lawler, "Aberration-corrected echelle spectrometer for measuring ultraviolet branching fractions of iron-group ions," Appl. Opt. **51**, 8407–8412 (2012).

4. K. Robert and A. Roland, "Enhancing precision in fs-laser material processing by simultaneous spatial and temporal focusing," Light Sci. Appl. **3**, e169 (2014).
5. O. Furxhi, L. M. Daniel, and J. B. David, "Echelle crossed grating millimeter wave beam scanner," Opt. Express **22**, 16393–16407 (2014).
6. Y. T. Zhu, X. H. Wu, and W. Lei, "High resolution spectrograph with R4 echelle for LAMOST," Proc. SPIE **5492**, 401–409 (2004).
7. M. J. Porter, "Spectroscopy on small telescopes: the echelle spectrograph," Astrophys. Space Sci. **273**, 217–224 (2000).
8. T. Sakanoi, Y. Kasaba, and M. Kagitani, "Development of infrared Echelle spectrograph and mid-infrared heterodyne spectrometer on a small telescope at Haleakala, Hawaii for planetary observation," Proc. SPIE **9147**, 91478D (2014).
9. F. Pascal, D. Menut, and R. Brennetot, "Analysis by laser-induced breakdown spectroscopy of complex solids, liquids, and powders with an echelle spectrometer," Appl. Opt. **42**, 6029–6035 (2003).
10. N. Eddy, C. V. Ann, D. Rachel, and R. T. Ian, "NOMAD spectrometer on the ExoMars trace gas orbiter mission: part 1-design, manufacturing and testing of the infrared channels," Appl. Opt. **54**, 8494–8520 (2015).
11. D. L. Miller and A. Scheeline, "A computer program for the collection, reduction and analysis of echelle spectra," Spectrochim. Acta Part B **48**, E1053–E1062 (1993).
12. F. L. Moore and F. Benjamin, "Echelle calibration and wavelength calculation," J. Opt. Soc. Am. **62**, 762–766 (1972).
13. D. A. Sadler and D. Littlejohn, "Automatic wavelength calibration procedure for use with an optical spectrometer and array detector," J. Anal. At. Spectrom. **10**, 253–257 (1995).
14. F. Jonh, L. J. Richard, and H. C. Jack, "Temperature and pressure variation of the refractive index of diamond," Appl. Opt. **16**, 2949–2951 (1977).
15. T. Arnold and R. Henry, "Estimating effects of temperature and moisture on C^2_n in the damp unstable boundary layer for visible, infrared, radio, and millimeter wavelengths," Proc. SPIE **1688**, 465–476 (1992).
16. L. M. Surhone, M. T. Tennoe, and S. F. Henssonow, *Cauchy's Equation* (Betascript, 2010), p. 125.
17. C. Chen, G. Wang, X. Wang, Y. Zhu, Z. Xu, T. Kanai, and S. Watanabe, "Improved Sellmeier equations and phase-matching characteristics in deep-ultraviolet region of KBe_2BO_3F crystal," IEEE J. Quantum Electron. **44**, 617–621 (2008).
18. N. Yokoi and Y. Aizu, "Methods for measuring refractive index and absorption coefficient of a moving particle using polarized-type phase-Doppler technique," Measurement **42**, 1352–1362 (2009).

159.226.165.13 {ts '2017-06-23 01:49:11'}